steel research international
www.steel-research.de

Influence of Quenching and Partitioning on the Mechanical Properties of Low-Silicon 33MnCrB5 Boron Steel

Silvia Barella, Marco Belfi, Andrea Gruttadauria, Pietro Cetto, Caiyi Liu, and Yan Peng*

Quenching and partitioning (QP) is a heat treatment that is designed to enhance both the mechanical properties and ductility of low- and medium-carbon steels. This treatment is performed on steels with a tailored chemical composition. Herein, QP treatments are designed and performed on commercial low-silicon 33MnCrB5 boron steel. Different temperatures (evaluated using thermodynamic simulations) and times are tested. Scanning electron microscopy investigations are conducted to observe the microstructure, whereas X-ray diffraction and electron backscattered diffraction analyses are performed to assess the presence and amount of retained austenite (RA). Tensile tests are performed to investigate the mechanical properties. The designed treatments introduce a fraction of up to 4.6% of RA in the final microstructure. Tensile tests show that the QP samples are characterized by high ultimate tensile strength (1633–1756 MPa) with an increased elongation at break with respect to the reference quenching and tempering condition (16–18% versus 9%). Hardening coefficients are linked to martensite tempering in the initial stages of plastic deformation, whereas at higher strains, they are mostly influenced by RA presence. The proposed treatments are successfully performed on 33MnCrB5 grade, leading to a set of tensile properties that are not exploitable with traditional treatments.

1. Introduction

Quenching and partitioning (QP) is a heat treatment first proposed by Speer et al., which has the aim to obtain a microstructure composed of martensite and retained austenite (RA), whose presence modifies the final properties of the material itself.[1–5] It must be noted that the presence of this soft phase inside the microstructure not only increases the ductility but also provides high mechanical properties; when subjected to a load, it undergoes a strain-induced transformation into martensite, which also increases the ultimate tensile strength (UTS). The presence of RA should be tailored to achieve the desired mechanical properties of the final material.[6–9] Moreover, it must be noticed that, depending on the morphology and stability of austenitic particles, and on the surrounding microstructure, different strain-induced transformation kinetics are obtained, thus introducing different properties in the material.[10–12] Several studies have shown that the final properties obtained through this treatment, depending on the steel grade, can reach an UTS of 1600–2000 MPa associated with good values of elongation at break: these properties are not achieved with traditional quenching and tempering (QT) treatments.[6,13,14] QP has usually been applied only to laboratory compositions, tailored to optimize the outcome of the treatment, since the composition of alloy is crucial to achieve the desired results. As the whole process is based on carbon diffusion indeed, a higher carbon concentration theoretically increases the amount of RA that could be stabilized. However, carbon is involved in competing mechanisms as carbide precipitation, which reduces the overall amount of carbon effectively diffusing into austenite; the control of carbides formation is one of the key features which can lead to an effective QP treatment.[15,16] Several studies have observed that the addition of elements such as Si (and Al with less effect) can slow down the kinetics of carbides precipitation, helping partitioning process. An amount of silicon of at least 1.5% wt. is enough to control carbide formation. However, silicon is often an undesired element in the industry at these high concentrations; therefore, commercial steels usually have a lower amount in their

S. Barella, M. Belfi, A. Gruttadauria, P. Cetto
Dipartimento di Meccanica
Politecnico di Milano
via la Masa 1, 20156 Milano, Italy
E-mail: marco.belfi@polimi.it

C. Liu, Y. Peng
National Engineering Research Center for Equipment and Technology of Cold Rolled Strip
Yanshan University
No. 438 West Section of Hebei Street, Qinhuangdao 066004, Hebei
P. R. China

The ORCID identification number(s) for the author(s) of this article can be found under https://doi.org/10.1002/srin.202300622.

DOI: 10.1002/srin.202300622

composition.[16–20] For example, some tailored compositions for QP treatments (QP980, QP1180) show Mn and Si amounts which are rarely produced in the industry as commercial grades.[21,22]

As a consequence, new interest is focused on the application of QP on commercial alloys, which are featured by a composition which has not been designed precisely for this treatment, but are already used in the industry: the effective application of such a treatment can be proposed as a new path to obtain high mechanical properties with enhanced ductility with respect to QT. Some QP treatments have been performed on 22MnB5 boron steel for hot stamping, both in the standard version[23,24] and in a high-Si one,[25] showing the possibility to exploit this treatment on this class of materials with interesting results: in particular, the former two have produced UTS values of 1400–1700 Mpa, coupled with A% in the range of 10–13%.

The treatment consists of full austenitization, followed by quenching at a temperature between M_s and M_f, which leaves a martensitic microstructure with some austenite. Then, an isothermal holding at the same temperature of quenching or at a temperature just above M_s, the partitioning step, allows the stabilization of austenite through the diffusion of carbon from the supersaturated martensite to the austenite itself.[1,26] If partitioning is performed at the quenching temperature, the treatment is called "single step", whereas in the second case, it is called "double step".[13,14,17,26] Finally, the material is water quenched: during this operation, a fraction of austenite that has not been stabilized transforms into "fresh martensite" (FM), whereas another part, which is stable at room temperature, is called RA.[2,27]

Two parameters must be taken into account. In the design of QP: quenching temperature (QT) and the partitioning time (t_p) must be taken into account. The former defines the martensitic–austenitic-mixed microstructure: as the formation of martensite is a military operation, the amount of phases obtained through quenching depends on selected quenching temperature. The latter is the period in which carbon diffuses from supersaturated martensite to austenite to stabilize it. As the partitioning is diffusion based, the combination of temperature (PT) and time (t_p) is pivotal for obtaining the desired microstructure: some studies have highlighted that the amount of austenite is widely influenced by these parameters as some competing mechanisms can activate during time exposure.[16,28–30] RA stability is also deeply influenced by the heat treatment.[20,31] Therefore the selection of PT and t_p can generate very different sets of tensile properties.[13,25,32]

Speer et al. first proposed the carbon-constrained equilibrium (CCE) theoretical model that was implemented to design the first guess optimal partitioning temperature.[1,33] The CCE model is based on three hypotheses: only carbon diffusion is considered; carbon entirely diffuses from martensite to austenite without forming carbides, and a fixed interface is present.

CCE is computed starting from the estimation of the initial amounts of martensite and austenite after quenching at a certain temperature QT between M_s and M_f, given by the Koistinen Marburger equation (Equation (1)).

$$f_m = 1 - e^{[-K(M_s - QT)]} \tag{1}$$

This equation is coupled with the mass balance of carbon between the different fractions f_i of martensite (α) and austenite (γ) and the overall carbon concentration X_c.

$$f^{\alpha}_{CPE}(1 - X^{\gamma}_{C_{CPE}}) = f^{\gamma}_{i}(1 - X^{alloy}_{C}) \tag{2}$$

Using the carbon balance and the relationship between the fractions of the two phases (Equation (3) and (4))

$$f^{\alpha}_{CPE}X^{\alpha}_{C_{CPE}} + f^{\gamma}_{CPE}X^{\gamma}_{C_{CPE}} = X^{alloy}_{C} \tag{3}$$

$$f^{\alpha}_{CPE} + f^{\gamma}_{CPE} = 1 \tag{4}$$

By those relationships, the computation about the final fractions of the two different phases after complete partitioning is possible. Through these equations it is therefore possible to have a preliminary theoretical estimation of the optimal quenching temperature to maximize the final amount of RA.

This study focuses on the design and application of QP on an already existing commercial alloy featured by a composition that has not been tailored for this heat treatment. Grade 33MnCrB5 is a low-silicon boron steel which is commonly used in quenched condition for agricultural components and in the QT condition for bolts. The selected steel is a medium-carbon steel featured by the presence of manganese, chromium, and boron as alloying elements. Manganese is an austenitizing element, so it widens the existence field for austenite, and it supports the hardening process. Chromium is a ferritizing element which forms carbides in steels, whereas small boron additions enhance the strength of the material.[34] Titanium is also present and it can precipitate into carbides that are reported to enhance mechanical properties of steel.[35] Moreover, the alloy is featured by a low amount of silicon, leading to an increased complexity in the design of the partitioning treatment, as carbides precipitation is not controlled.

The goal of the study is to design and perform QP treatments on this commercial alloy and to verify the effect of such a treatment on the tensile properties of the treated material, in order to evaluate feasibility of this treatment on commercial 33MnCrB5 steel.

2. Experimental Section

The chemical composition of the analyzed steel is reported in **Table 1**.

QP treatments were performed using muffle ovens; for the partitioning treatments, salt baths composed of a commercial mixture of nitrites and nitrates were used. Scanning electron microscopy (SEM) and electron backscattered diffraction (EBSD) analyses were done using Zeiss EVO 50. Tensile tests were conducted with a MTS100 machine, with 2 mm min^{-1} crosshead speed and initial gauge length of 50 mm, on nonproportional cylindrical samples with a 7 mm diameter. Two samples per each condition were tested.

Critical temperatures and time range for the treatments were computed through Thermocalc 2023a, using the equilibrium

Table 1. Steel chemical composition.

Element	C	Mn	Cr	Si	B	Ti	S	P	Fe
wt%	0.32	1.27	0.33	0.19	0.0025	0.043	0.001	0.01	Balance

calculator and the martensite model. The modeling of carbon diffusion from martensite to austenite during partitioning was performed through DICTRA extension embedded in the software, which is based on CALPHAD approach and the numerical solution of the multicomponent diffusion equations.

The parameters featuring heat treatments are reported in **Table 2**:

All the heat treatments were performed after austenitization of 7 min at 850 °C, as reported in **Figure 1**. The austenitization temperature was chosen in a consistent manner with the industrial practice, which was 50/70 °C above the critical point A_3.

X-ray diffraction (XRD) analyses were performed through a Rigaku SmartLab SE using a D/Tex Ultra 250 as a detector. X-ray worked at 40 kV and 40 mA, with a Cu Kβ filter 1D. Scan range went from 35° to 120° with step size of 0.02° and a scan speed of 0.5° min^{-1}. Rietveld analysis was performed on the integrated software Smartlab Studio II. Rectangular specimens (7 mm × 20 mm × 5 mm) were used.

SEM analyses were performed using a Carl Zeiss EVO 50 equipped with field emission gun (FEG), on specimen etched with Nital 2% solution, to highlight the microstructure. EBSD analyses were done to investigate the presence of RA: specimens were smoothly polished using silica gel to obtain a smooth surface.

3. Results

Critical temperatures computed through thermodynamic simulation are shown in **Table 3**:

Table 2. Partitioning treatments parameters.

Sample	QT [°C]	t_p [min]
240-5	240	5
240-10	240	10
260-5	260	5
260-10	260	10

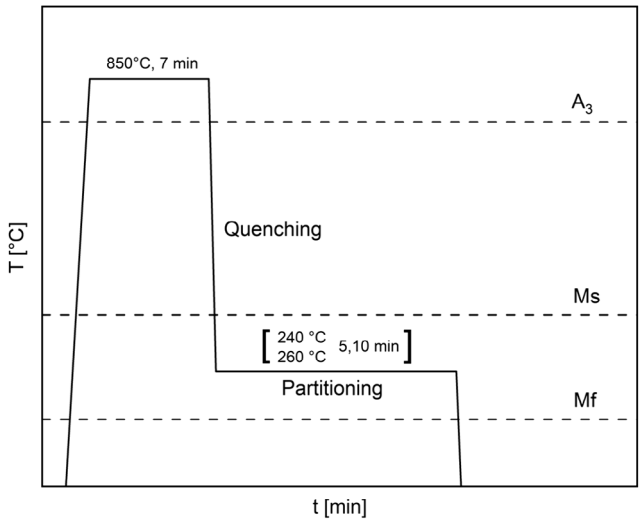

Figure 1. Design of quenching and partitioning treatments.

Table 3. Critical temperatures.

Critical temperatures [°C]	
M_s	347
M_f	221
A_1	703
A_3	784

Koistinen–Marburger law, recently modified by Lee and Van Tyne, is used to calculate the amount of austenite transformed into martensite during quenching.[36] This rule has also been used for CCE modeling to establish the maximum amount of RA that could be theoretically stabilized through partitioning (**Figure 2**).

However, this is a first approximation; because the partitioning time is not enough to complete the process, carbides precipitation is not considered and the austenite/martensite interface is not fixed, so the estimation of the optimal quenching temperature (257 °C) was used here as a first guess for the design of the experimental trials. Two different temperatures (240, 260 °C) were selected to account for the deviations from the theoretical model expected in actual experiments.[30]Time ranges for the treatments were selected through DICTRA diffusion simulation, which was used to predict carbon diffusion from the supersaturated martensitic matrix to unstable austenite during partitioning. Following the result of CCE presented in Figure 2, the temperature was set to 260 °C. The goal was to establish a range for the times in which stabilization of film RA, which is typically submicrometric, is obtained.[37] The initial condition is taken as immediately following the first quenching, in which austenite and martensite have the same initial composition, which is the alloy composition. The model is 1D and analyzes the carbon diffusion process from the supersaturated martensite to austenite during partitioning, for increasing times. Stability is achieved when the carbon concentration in RA is enough to move from M_s to room temperature. M_s was computed through the

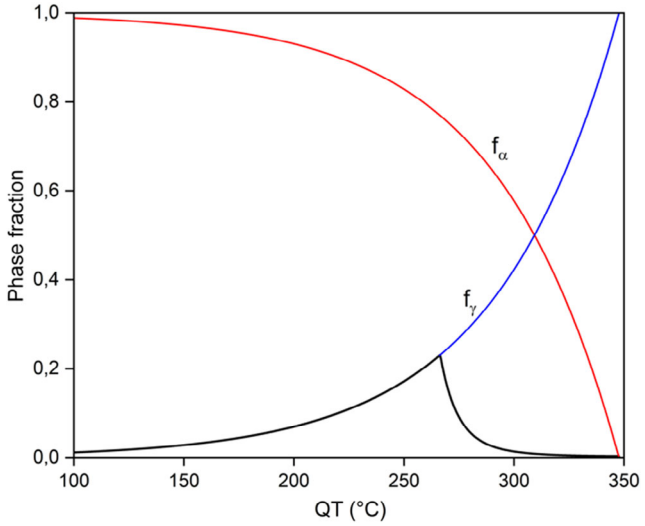

Figure 2. CCE model computation.

composition-based equation developed by Capdevila et al.[38] While 1 min partitioning can stabilize austenite only until a width lower than 0.1 μm, 5 and 10 min are enough to obtain higher width (0.12–0.4 μm), as shown in **Figure 3**A. Moreover, a preliminary evaluation of the variation of the stabilized width as a function of partitioning time was performed. As shown in Figure 3B, the increase in the stabilized austenite width with respect to the partitioning time ($\Delta w_s/\Delta t_p$) decreases with increasing partitioning time, meaning that the effectiveness of stabilization is higher in the first stages: increasing t_p doesn't lead to a proportional stabilized width. Therefore, it is concluded that 5–10 min of partitioning are enough to stabilize fine RA, and thus they are selected for the treatments.

The microstructure is characterized by acicular-shaped martensite (**Figure 4**), as expected after quenching on a steel with such a carbon concentration, while austenite is hardly detectable at these magnifications. No major differences have been observed among the different samples, as the features of austenite-to-martensite transformation are influenced just by the carbon concentration.

XRD has been performed to detect the presence of RA at room temperature after the heat treatments.

RA presence has been detected in all the specimens, as γ-phase peaks are present in all the spectra shown in **Figure 5**. Rietveld analysis has been performed in order to quantify the amount of the phases: the amount of RA obtained is between 2.6 and 4.6% (**Table 4**).

The amount of RA is low (2.6–4.6%) and very similar between all the different cases. The highest amount of RA (4.6%) was observed in the sample treated at 240 °C for 5 min.

EBSD analyses have been employed to detect the presence of FCC RA into the martensite matrix.

The results of the phase maps, presented for 240-5 and 240-10 case (**Figure 6**), point out the presence of RA into the microstructure. The stabilized austenite is present in fine dispersion, and its dimension is submicrometric, as expected also according to literature.[37,39] Carbon diffusion is responsible for austenite stabilization, and it is a phenomenon governed by temperature and time; therefore, RA is usually found in thin regions because at these low temperatures and time values, the carbon diffusion might stabilize austenite at a limited distance from martensite, as expected from literature and simulation.[37]

Tensile tests have been performed to address the effect of QP treatments on the mechanical properties of the investigated alloy. A comparative sample (240-10-QT), subjected to QT treatment (240 °C, 10 min), was designed. This condition has been selected as the reference value for comparing the results obtained for QP-treated samples. The tempering parameters were selected to be identical to the partitioning step of 240-10 sample: the choice was made to have the same level of martensite tempering in order to highlight the effect of the presence of residual austenite as a discriminant between the two conditions.

The results are reported in **Table 5**.

Tensile properties of the QP samples show very high UTS values, ranging between 1633 and 1756 MPa. It can be observed in **Figure 7** that with increasing tempering level, UTS is progressively reduced. These UTS values are comparable to the QT-240-10 case, as expected due to the presence of a martensitic matrix characterized by the same tempering level. Nevertheless, an important difference is obtained regarding YS, which changes from 1467 MPa of the QT condition to 991–1153 MPa of the QP conditions. As a result, the ratio between the UTS and the YS appears to be higher. This effect is related to the presence of ductile RA into the microstructure, while the QT condition, which is featured by no presence of RA, shows the lowest ratio.

Focusing on the direct comparison between 240-10 and 240-10-QT samples, **Figure 8** highlights the incremental effect of RA on the ductility of the material. Elongation at break indeed is the parameter most influenced by heat treatment: QP shows a value that is almost double of the QT (17% versus 9%). As a consequence, the analysis of hardening coefficients was performed to provide evidence of the occurrence of TRansformed-Induced Plasticity (TRIP) effect during the tensile test, which leads to the delay of necking, increasing the elongation. Hardening coefficients "*n*" were calculated for the different cases using the relation

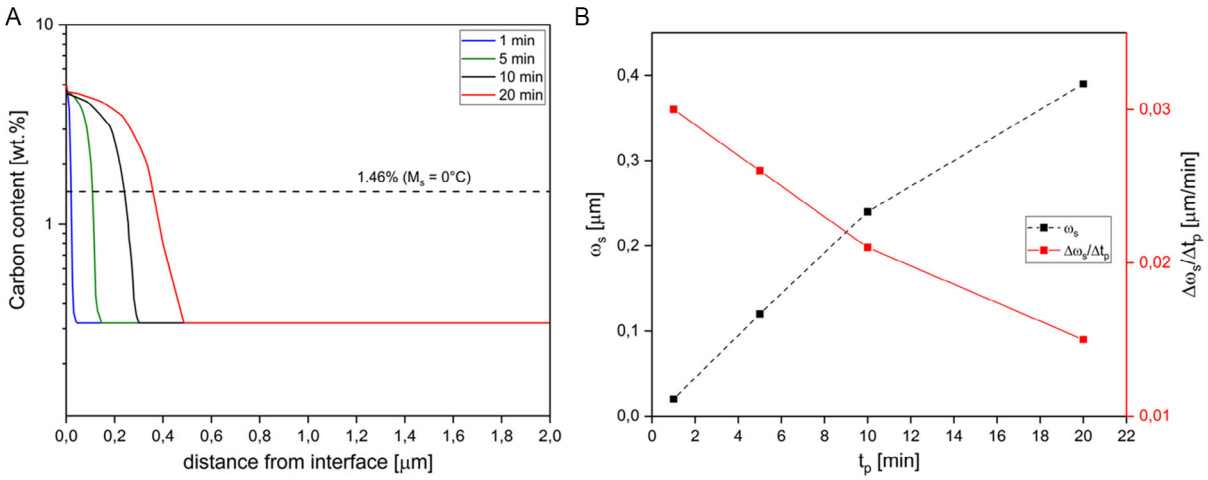

Figure 3. A) Carbon profile evolution in austenite during partitioning and B) evolution of w_s and $\Delta w_s/\Delta t_p$ along partitioning.

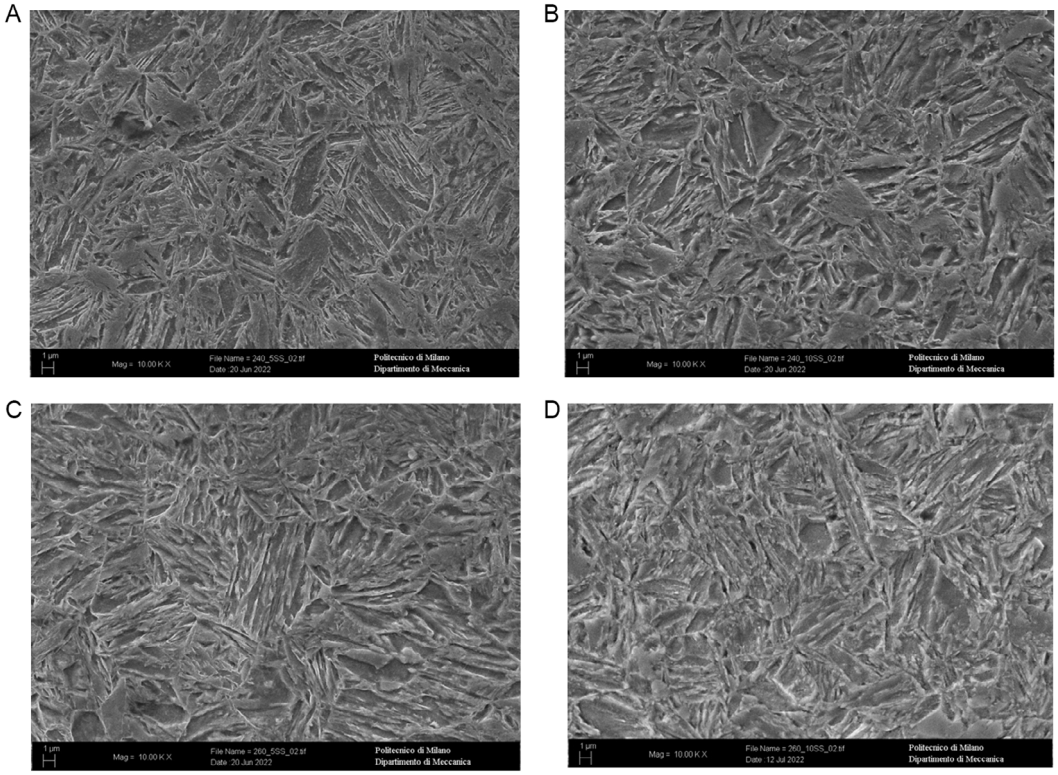

Figure 4. SEM images of the microstructure: A) 240-5, B) 240-10, C) 260-5, and D) 260-10.

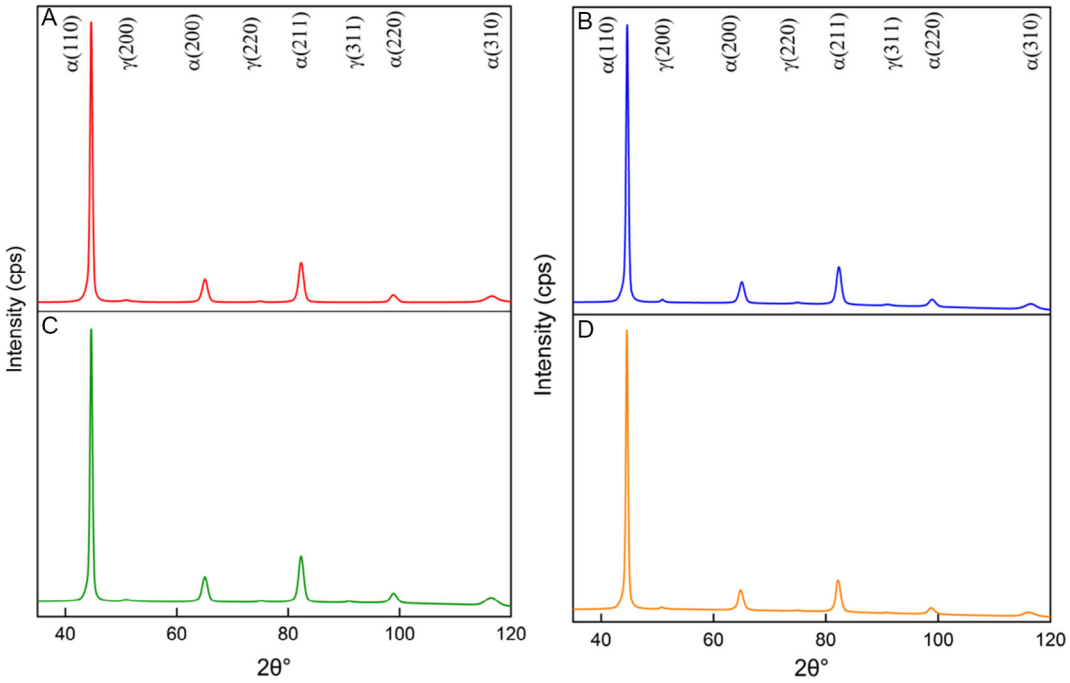

Figure 5. XRD spectra: A) 240-5, B) 240-10, C) 260-5, and D) 260-10.

Table 4. RA amounts detected in the treated samples.

Sample	RA [%]
240-5	4.6
240-10	3.1
260-5	4.3
260-10	2.6

Table 5. Tensile properties' recap for the different conditions.

Sample	YS [MPa]	UTS [MPa]	*A* [%]	UTS/YS
240-5	991 ± 21	1756 ± 22	18	1.77
240-10	1043 ± 16	1740 ± 14	17	1.68
260-5	1021 ± 7	1687 ± 3	16	1.65
260-10	1153 ± 18	1633 ± 12	17	1.42
240-10-QT	1461 ± 5	1723 ± 9	9	1.16

$$\sigma = K\varepsilon^n \tag{5}$$

σ and ε are true stress and strain, respectively, computed in the range between YS and UTS.

Hardening coefficient is obtained from Equation (6).

$$n = \tan\frac{\log(\sigma)}{\log(\varepsilon)} \tag{6}$$

It can be observed that the hardening coefficient is equal to the derivative of the curve in the $\log(\sigma)-\log(\varepsilon)$ plot (**Figure 9**). As a consequence, a progressive decrease in the hardening coefficients can be observed, which means that the material decreases its hardening effect as deformation increases.

These considerations can also be discussed through the computation of the instantaneous hardening coefficient for the different cases (**Figure 10**). Its value decreases for all the different cases as the plastic deformation process progresses: in the very first stages, the values of the instantaneous hardening coefficients range from 0.39 to 0.49 and then progressively decrease to values lower than 0.1. These values are comparable to the ones found in literature for QP and TRIP steels.[40,41] Findley et al. observed that the initial instantaneous hardening coefficients are mostly related to the state of the martensitic matrix, as an increasing tempering level decreases the initial value of n.[42] In Figure 9, the highest initial n value is observed in the 240-5 case, while the lowest is observed in the 260-10 case. Moreover, the QT sample confirms these considerations, as its initial value is comparable to the 240-10 sample: a similar martensite tempering obtained in one case through partitioning, while in the other through tempering results in similar initial hardening coefficients (0.42, 0.43).

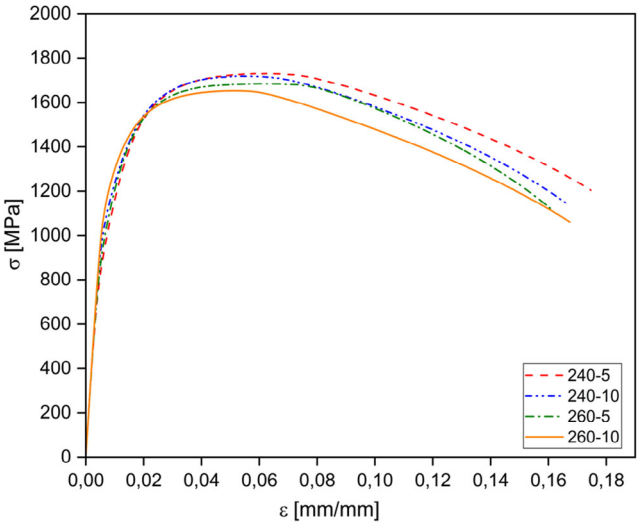

Figure 7. Tensile tests.

The effect of RA instead is more significant for higher deformation levels. While martensite hardenability reaches saturation, RA absorbs energy through plastic deformation and strain-induced transformation, delaying necking for higher strains. The transformation starts from the least stable austenite grains and moves to more stable ones. As a consequence, the uniform elongation stretch is increased by the presence of stable

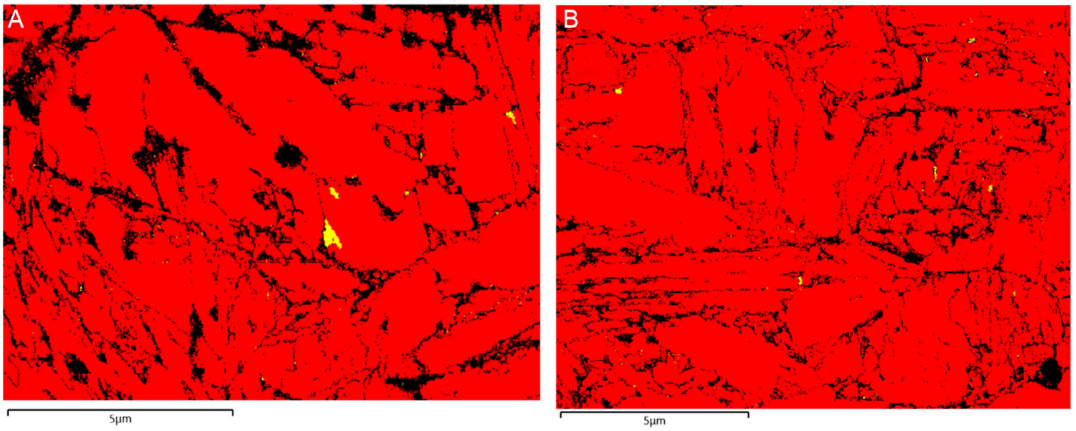

Figure 6. Phase maps. A) 240-5 on the left and B) 240-10 on the right. Austenite in yellow. Martensite in red.

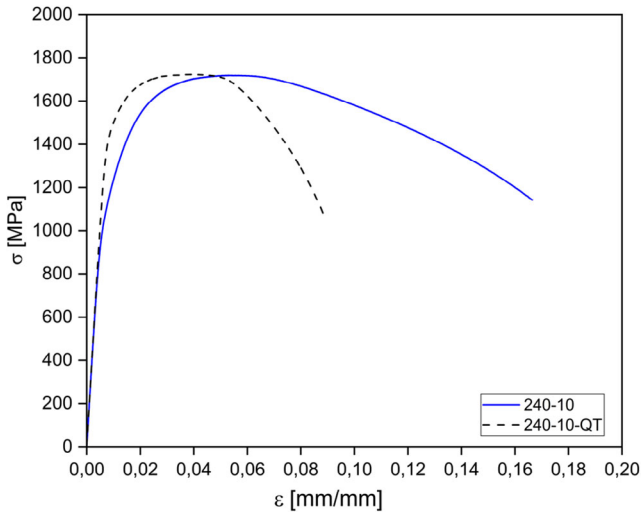

Figure 8. 240-10 (QP) and 240-10-QT tensile properties comparison.

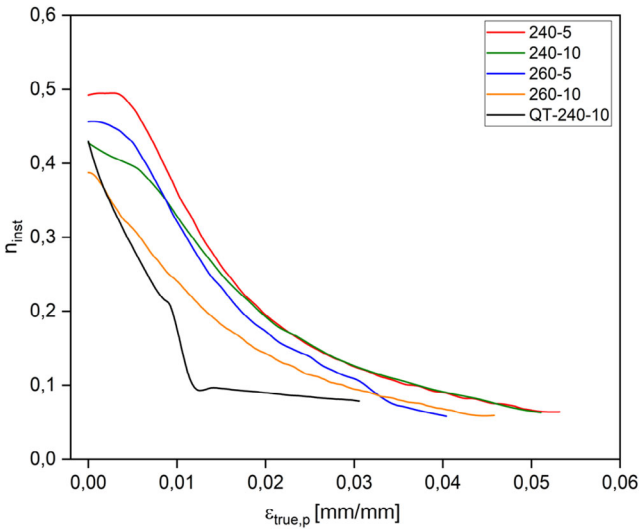

Figure 10. Instantaneous hardening coefficient comparison.

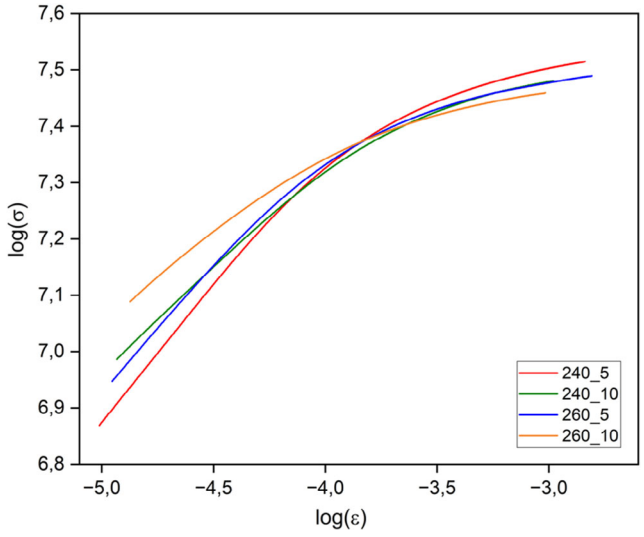

Figure 9. $\log(\sigma) - \log(\varepsilon)$ plot.

RA at higher strains: QP samples exploit this effect, showing in Figure 9 increased $\varepsilon_{true,pl}$ (0.041–0.053) compared to the QT condition (0.031).

4. Discussion

The design and application of QP on 33MnCrB5 has led to the stabilization of a fraction of RA in a martensitic microstructure, so it can be stated that the treatment has been carried out successfully. SEM analysis has confirmed that the microstructure is martensitic, while XRD and EBSD have independently demonstrated that an amount of RA is present at room temperature. The latter in particular has shown that its morphology and dimension vary within the microstructure, as both blocky and interlath particles were detected: it's reported in literature that the latter condition is more desirable to exploit its effect on the increase of ductility of the material.[10,43] In both cases, its dimensions are less than micrometric, and especially for interlath morphology, its detection is difficult even at high magnification.[37]

The amount of RA detected is between 2.6% and 4.6%, which is lower than the one predicted by the CCE model (Figure 2); however, as the hypothesis of the theoretical model is not fulfilled in real experiments,[44] this difference in RA amount is explained, as suggested by Bigg et al. as well.[25] Especially, the low amount of silicon in the alloy (0.19%) does not allow control of carbide precipitation and thus leads to lower partitioning efficiency with respect to higher silicon grades.[16] In other steels with a similar amount of carbon, this partitioning time has also been observed as suitable to obtain good end results[14]; the same has happened in another Si-enriched boron steel.[25]

In any case, even such a low quantity seems enough to deeply influence the final tensile properties, as the different conditions show very high UTS (1633–1756 MPa). A comparison QT condition was developed, characterized by a tempering treatment performed at the same time and temperature as the partitioning (240 °C, 10 min), in order to obtain a microstructure featured by the same martensite tempering of the corresponding QP sample 240-10, but without RA: the measured UTS of QT-240-10 is comparable with the corresponding QP 240-10 (Figure 8). Nevertheless, the effect of RA is shown by the increased *A*% of the QP samples, which reaches 16–18%, with respect to 9% of the QT condition. In addition, the ratio UTS/YS, which is linked to the hardening capability of the material, is also increased in a substantial way in QP conditions, showing the exploitation of strain-induced transformation of austenite during straining. These properties are featured by a higher elongation with respect to the ones observed by Kong et al., and Liu et al. for a 22MnB5 boron steel[24,45] and for a B1500HS boron steel.[23] QP indeed allows the achievement of a new set of properties, which are not exploitable through traditional treatments.

Some other considerations can also be drawn while analyzing the stress–strain curves. RA is a soft phase, so it increases the

ductility of the alloy delaying necking, and moreover it transforms mechanically into martensite through the so-called TRIP effect when subjected to deformation.[20,46,47] This can allow the material to exploit high mechanical properties coupled with increased ductility.

As shown in Figure 9, the initial hardening coefficients are high (0.38–0.49) both in QP and in QT samples. This behavior is coherent with the observations of Findley et al.[42] which proved that the initial values of the work hardening coefficients are mostly related to the level of tempering of the martensitic matrix: a less-tempered martensite shows a higher hardening coefficient than a more tempered one. In this case indeed, 240-5 sample shows a higher initial hardening coefficient than 260-10 sample, while the comparative QT condition and 240-10 QP condition, featured by same martensite tempering, show the same starting value. Coherently with the previous discussion, the instantaneous hardening coefficient smoothly decreases asymptotically to the characteristic values of QT, leading to the conclusion that strain-induced transformation occurs progressively during the plastic deformation process. The transformation starts from the less stable austenite particles and moves to the more stable ones for increasing strain.[37,48] Strain-induced transformation indeed slows down the decrease of the hardening coefficient as undeformed FM, featured by a high hardening coefficient, is progressively formed[49]: the decrease of the hardening coefficient becomes thus smooth, and necking is delayed. The trend observed is similar to the one observed by De Moor et al.[41] and, with a different representation, Finfrock et al.[45] for QP steels.[46] The observed evolution in the instantaneous hardening coefficient is slightly different from the one found for TRIP steels by Saeidi et al.[40] and Finfrock et al.,[50] where an increase of the hardening coefficient at a later stage of deformation was observed. The strain hardening dynamics observed here are more similar to the ones found in literature for DP steels by He et al.[51] and by Chiang et al. for TRIP steels.[11] The presence of two stages of deformation, featured by different hardening coefficients, has been observed in different cases for multiphase microstructures such as dual-phase triphase and ferritic–bainitic dual-phase steels.[52–54]

Finally, 33MnCrB5 commercial steel, not specifically designed for QP, can be used for such a treatment, showing enhanced performances with respect to the conventional condition.

5. Conclusion

Different single-step QP treatments have been successfully performed on commercial low-silicon 33MnCrB5 boron steel. The following conclusions can be drawn. 1) The designed treatments can effectively stabilize a fraction of fine RA in 33MnCrB5 steel into the martensitic microstructure. 2) UTS values ranging from 1633 to 1756 MPa are obtained, coupled with higher A% with respect to the comparative QT sample, featured by similar martensite tempering (16–18% versus 9%). 3) Initial hardening coefficient is mostly related to the state of the martensitic matrix: 240-5 sample shows the highest value, while 260-10 the lowest. QT comparative sample is featured by similar initial hardening coefficient, as expected by the presence of a martensitic matrix characterized by the same tempering. 4) Uniform elongation stretch between YS and UTS is increased in QP samples by the presence of RA which, through the progressive exploitation of the strain-induced transformation, delays the occurrence of necking.

Acknowledgements

There are no additional acknowledgements associated with this article.

Conflict of Interest

The authors declare no conflict of interest.

Data Availability Statement

The data that support the findings of this study are available from the corresponding author upon reasonable request.

Keywords

boron steels, low-silicon steels, quenching and partitioning, strain-induced transformations, tensile properties

Received: September 18, 2023
Revised: November 23, 2023
Published online:

[1] J. Speer, D. K. Matlock, B. C. De Cooman, J. G. Schroth, *Acta Mater.* **2003**, *51*, 2611.
[2] J. G. Speer, E. De Moor, K. O. Findley, D. K. Matlock, B. C. De Cooman, D. V. Edmonds, *Metall. Mater. Trans. A* **2011**, *42*, 3591.
[3] J. G. Speer, E. De Moor, A. J. Clarke, *Mater. Sci. Technol.* **2015**, *31*, 3.
[4] O. Matsumura, Y. Sakuma, Y. Ishii, J. Zha, *ISIJ Int.* **1992**, *32*, 1110.
[5] E. De Moor, J. G. Speer, D. K. Matlock, D. N. Hanlon, in *MS and T'11*, Columbus, OH, October **2011**, pp. 568–579.
[6] M. Liu, J. Wang, Q. Zhang, H. Hu, G. Xu, *Met. Mater. Int.* **2021**, *27*, 2473.
[7] V. Kurup, C. Siyayisa, R. Mostert, J. Moema, *S.-Afr. Tydskr. Natuurwet. Tegnol.* **2022**, *40*, 102.
[8] L. Kucerova, D. Aisman, H. Jirkova, B. Masek, D. Hauserova, in *The 20th Int. DAAM World Symp.*, Wien, November **2009**, pp. 1035–1036.
[9] B. B. He, M. Wang, M. X. Huang, *Metall. Mater. Trans. A* **2019**, *50*, 4021.
[10] G. N. Haidemenopoulos, N. Aravas, I. Bellas, *Mater. Sci. Eng., A* **2014**, *615*, 416.
[11] J. Chiang, B. Lawrence, J. D. Boyd, A. K. Pilkey, *Mater. Sci. Eng., A* **2011**, *528*, 4516.
[12] A. Kozłowska, A. Janik, K. Radwański, A. Grajcar, *Materials* **2019**, *12*, 3042.
[13] H. Jirková, L. Kučerová, B. Mašek, *Mater. Sci. Forum* **2012**, *706–709*, 2734.
[14] A. Kumar, V. K. Sharma, A. K. Sharma, S. K. Biswas, S. Kumar, K. Muraleedharan, *Mater. Res. Express* **2018**, *5*, 116503.
[15] F. HajyAkbary, J. Sietsma, G. Miyamoto, T. Furuhara, M. J. Santofimia, *Acta Mater.* **2016**, *104*, 72.
[16] I. Miettunen, S. Ghosh, M. C. Somani, S. Pallaspuro, J. Kömi, *J. Mater. Res. Technol.* **2021**, *11*, 1045.
[17] J. Vorel, I. Jenicek, S. Kana, *J. Phys.: Conf. Ser.* **2016**, *755*, 011001.
[18] B. Kim, J. Sietsma, M. J. Santofimia, *Mater. Des.* **2017**, *127*, 336.

[19] M. J. Santofimia, L. Zhao, R. Petrov, J. Sietsma, *Mater. Charact.* **2008**, *59*, 1758.
[20] S. Ebner, R. Schnitzer, E. Maawad, C. Suppan, C. Hofer, *Materialia* **2021**, *15*, 101033.
[21] M. Madrid, C. J. Van Tyne, S. Sriram, E. J. Pavlina, J. Hu, K. D. Clarke, *IOP Conf. Ser.: Mater. Sci. Eng.* **2018**, *418*, 012083.
[22] W. Guo, Z. Wan, P. Peng, Q. Jia, G. Zou, Y. Peng, *J. Mater. Process. Technol.* **2018**, *256*, 229.
[23] X. Han, Y. Zhong, P. Xin, Z. Cui, J. Chen, *Proc. Inst. Mech. Eng., Part B* **2017**, *231*, 1972.
[24] H. Kong, Q. Chao, M. H. Cai, E. J. Pavlina, B. Rolfe, P. D. Hodgson, H. Beladi, *Mater. Sci. Eng., A* **2017**, *707*, 538.
[25] M. Cheng, H. W. Song, X. Li, S. H. Zhang, M. Cheng, T. Lin, *Mater. Sci. Forum* **2014**, *788*, 340.
[26] H. Y. Li, X. W. Lu, W. J. Li, X. J. Jin, *Metall. Mater. Trans. A* **2010**, *41*, 1284.
[27] E. Paravicini Bagliani, M. J. Santofimia, L. Zhao, J. Sietsma, E. Anelli, *Mater. Sci. Eng., A* **2013**, *559*, 486.
[28] Y. Toji, G. Miyamoto, D. Raabe, *Acta Mater.* **2015**, *86*, 137.
[29] F. Peng, Y. Xu, J. Li, X. Gu, X. Wang, *Mater. Des.* **2019**, *181*, 107921.
[30] T. D. Bigg, D. K. Matlock, J. G. Speer, D. V. Edmonds, *Solid State Phenom.* **2011**, *172–174*, 827.
[31] S. Ebner, C. Suppan, A. Stark, R. Schnitzer, C. Hofer, *Mater. Des.* **2019**, *178*, 107862.
[32] M. Carpio, J. Calvo, O. García, J. P. Pedraza, J. M. Cabrera, *Metals* **2021**, *11*, 1136.
[33] J. G. Speer, F. C. Rizzo, D. K. Matlock, D. V. Edmonds, *Mater. Res.* **2005**, *8*, 417.
[34] S. N. Ghali, H. S. El-Faramawy, M. M. Eissa, *J. Miner. Mater. Charact. Eng.* **2012**, *11*, 1000.
[35] H. S. El-Faramawy, S. N. Ghali, M. M. Eissa, *J. Miner. Mater. Charact. Eng.* **2012**, *11*, 1108.
[36] S. J. Lee, C. J. Van Tyne, *Metall. Mater. Trans. A* **2012**, *43*, 422.
[37] C. Celada-Casero, C. Kwakernaak, J. Sietsma, M. J. Santofimia, *Mater. Des.* **2019**, *178*, 107847.
[38] C. Capdevila, F. G. Caballero, C. Garcia de Andres, *ISIJ Int.* **2002**, *42*. 894.
[39] M. J. Santofimia, L. Zhao, R. Petrov, C. Kwakernaak, W. G. Sloof, J. Sietsma, *Acta Mater.* **2011**, *59*, 6059.
[40] N. Saeidi, M. Jafari, F. Ashrafizadeh, M. Karimi, S. Ziaei-Rad, H. S. Kim, *Mater. Res. Express* **2018**, *5*, 126507.
[41] E. de Moor, S. Lacroix, A. J. Clarke, J. Penning, J. G. Speer, *Metall. Mater. Trans. A* **2008**, *39*, 2586.
[42] K. O. Findley, J. Hidalgo, R. M. Huizenga, M. J. Santofimia, *Mater. Des.* **2017**, *117*, 248.
[43] X. C. Xiong, B. Chen, M. X. Huang, J. F. Wang, L. Wang, *Scr. Mater.* **2013**, *68*, 321.
[44] M. J. Santofimia, L. Zhao, J. Sietsma, *Metall. Mater. Trans. A* **2011**, *42*, 3620.
[45] H. Liu, X. Lu, X. Jin, H. Dong, J. Shi, *Scr. Mater.* **2011**, *64*, 749.
[46] C. B. Finfrock, M. M. Thrun, D. Bhattacharya, T. J. Ballard, A. J. Clarke, K. D. Clarke, *Metall. Mater. Trans. A* **2021**, *52*, 928.
[47] M. Soleimani, A. Kalhor, H. Mirzadeh, *Mater. Sci. Eng., A* **2020**, *795*, 140023.
[48] P. J. Gibbs, E. De Moor, M. J. Merwin, B. Clausen, J. G. Speer, D. K. Matlock, *Metall. Mater. Trans. A* **2011**, *42*, 3691.
[49] D. S. Alves, D. G. Rodrigues, D. B. Santos, *Tecnol. Metal., Mater. Min.* **2022**, *19*, e2756.
[50] C. B. Finfrock, A. J. Clarke, G. A. Thomas, K. D. Clarke, *Metall. Mater. Trans. A* **2020**, *51*, 2025.
[51] Z. He, Y. He, Y. Ling, Q. Wu, Y. Gao, L. Li, *J. Mater. Process. Technol.* **2012**, *212*, 2141.
[52] A. Zare, A. Ekrami, *Mater. Sci. Eng., A* **2011**, *528*, 4422.
[53] A. P. Pierman, O. Bouaziz, T. Pardoen, P. J. Jacques, L. Brassart, *Acta Mater.* **2014**, *73*, 298.
[54] M. M. Karimi, S. Kheirandish, *Steel Res. Int.* **2009**, *80*, 160.